ACS APPLIED MATERIALS & INTERFACES

Research Article

www.acsami.org

Microwave-Assisted Chemical-Vapor-Induced in Situ Polymerization of Polyaniline Nanofibers on Graphite Electrode for High-Performance Supercapacitor

Xiaoqin Li,[†] Li Yang,[†] Ying Lei,[‡] Li Gu,[†] and Dan Xiao*[,†,‡]

[†]College of Chemistry and [‡]College of Chemical Engineering, Sichuan University, 29 Wangjiang Road, Chengdu 610064, PR China

Supporting Information

ABSTRACT: Polyaniline (PANI) nanofibers-coated graphite electrode is fabricated by microwave-assisted chemical vapor induced in situ polymerization in the presence of ammonium persulfate. The microstructure and electrochemical performance of the as-prepared nanofibers are investigated in detail. The obtained PANI nanofibers at the optimum volume ratio of 4% aniline, with some protuberances on the surface and the diameter from 50 to 100 nm, are coated onto the surface of graphite electrode. The PANI-coated graphite electrodes display the best electrochemical performance in 6 M H_2SO_4 electrolyte, including a large reversible capacity of 2136 F g^{-1} at the current density of 1 A g^{-1} and excellent rate capability. In particular, The PANI-coated graphite electrode exhibits a long cycle life by retaining 91% of the initial specific capacitance after 1000 cycles. More importantly, a symmetric supercapacitor was fabricated using PANI-coated graphite electrode, showing maximum energy density and power density of 24 Wh kg^{-1} and 6000 W kg^{-1}, respectively.

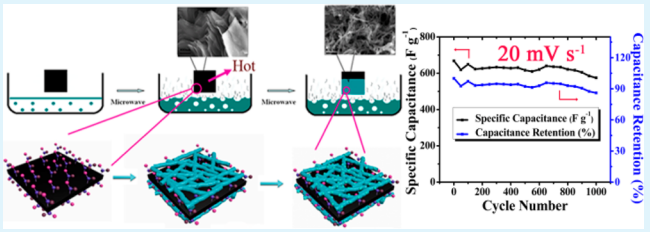

KEYWORDS: *polyaniline nanofibers, microwave-assisted chemical vapor, in situ polymerization, supercapacitor*

1. INTRODUCTION

With the increasing concerns about the environmental pollution and the rapid growth of portable electronics, there have been increasing demands of renewable and high-performance energy-storage devices. The rechargeable lithium batteries and electrochemical capacitors (ECs) are two of the most prominent alternatives in this respect.[1] On the basis of their energy storage mechanism, ECs can be categorized as two main subdivisions-electric double layer capacitors (EDLCs) and pseudocapacitors. EDLCs deliver relatively low specific capacitance (SC) due to their charge storage mechanisms based on reversible adsorption/desorption of ion at the electrode/electrolyte interface. However, pseudocapacitors display high SC associated with the fast and reversible redox reactions at/near the surface of active materials to generate capacitance, resulting them drawn much attention in recent years.[2] Among the reported pseudocapacitor materials,[3−5] conducting polymer has caught much attention because of its low energy optical transition, low ionization potential, and high electron affinity.

Polyaniline (PANI), as a conjugated polymer, has been considered as a promising EC material because of its low cost, easy synthesis, high specific capacitance, interesting redox behavior and good environmental stability.[6,7] The electron-conducting PANI has been demonstrated high electrochemical capacitance, resulting from the existence of multiple redox states in the presence of dopants. Scattered reports have investigated the performances of pure PANI capacitors by changing synthetic method[8] and dopants.[9] Among these reports, the moderate capacitances of the electrodes are not desirable and have great potential to be improved.

In recent works, some special morphologies of PANI have been synthesized, such as fibers/tubes,[10] flaky,[11] urchin-like,[12] and whisker-like.[13] In EC application, nanostructured PANI has greater SC and lower internal resistance relative to its conventional bulk counterpart due to higher effective surface area and shorter ion transport path.[14] Especially, the PANI nanofibers widely used in a number of fields have attracted growing attention because of their high aspect ratio, easy synthesis, and remarkable electrochemical properties.[8,9]

Several methods for preparing PANI nanofibers have been reported, including electrochemical polymerization and chemical oxidation polymerization.[15,16] In chemical oxidation polymerization, PANI nanofibers with diameters <100 nm can be made by template-guided polymerization[17] and adding surfactants.[18] However, these polymerization methods required amount of reaction time. Furthermore, the classical preparation process of working electrode by mixing PANI, binder and conductive agent, makes the procedures complex, although the binder is not necessary in some preparation process.[19,20] The addition of a binder (e.g., polyfluortetraethylene) into the working electrode in classical process impairs the electrical

Received: August 17, 2014
Accepted: October 31, 2014
Published: October 31, 2014

Scheme 1. Schematic Illustration of the Possible Formation Process of $PANI_1$-Coated Graphite Electrode under Microwave Radiation

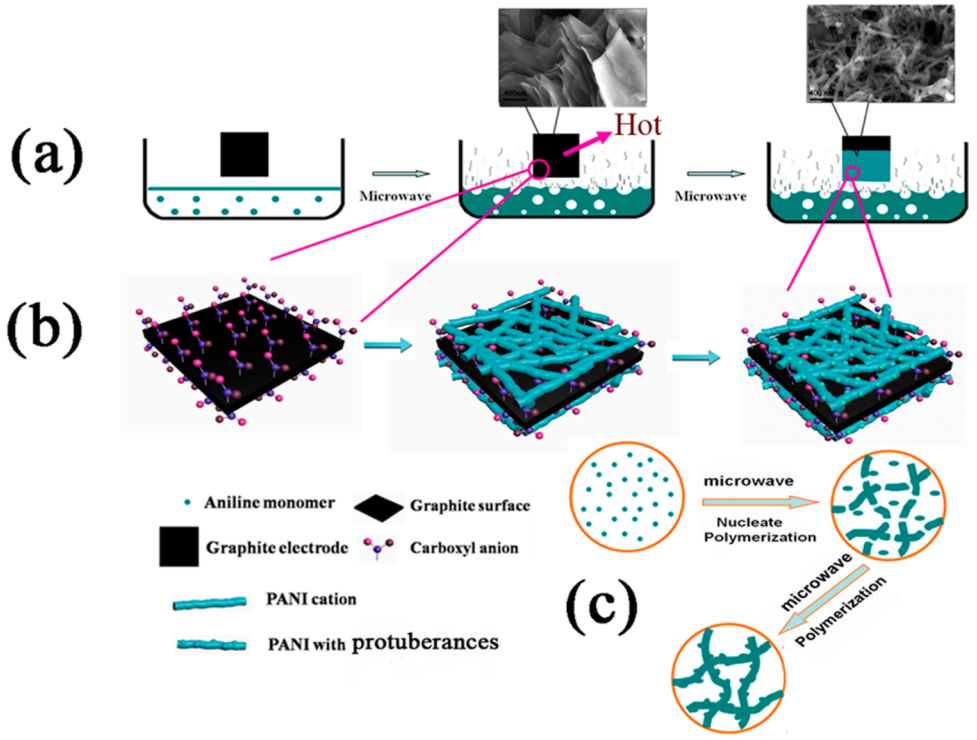

conductivity and increases the internal resistance of the working electrode.[21] Particularly noticeable, the in situ polymerization could complete through one-step reaction and obtain preferable purity products.[22] Several previous works have successfully synthesized PANI nanofibers in situ polymerization, indicating that the obtained PANI nanofibers show better electrochemical properties.[23]

In the present work, we adopted a fast microwave-assisted chemical vapor induced (MCVI) in situ polymerization method to successfully synthesize PANI on graphite electrode ($PANI_1$). The obtained $PANI_1$ was coarse nanofibrillar with diameter from 50 to 100 nm. The possible growth mechanism of the prepared $PANI_1$ nanofibers by in situ polymerization was revealed reasonably. This unique MCVI polymerization method not only made the procedures simpler, but also enhanced the electrochemical performance benefiting from the nanofibers structure and the special content of nitrogen in $PANI_1$. Herein, we investigated the effect of the concentration of electrolyte on the electrochemical properties of the $PANI_1$-coated graphite electrode by means of cyclic voltammetry (CV), galvanostatic charge−discharge and electrochemical impedance spectroscopy (EIS), indicating that the $PANI_1$-coated graphite electrode exhibited best electrochemical performance in 6 M H_2SO_4 electrolyte, including a large SC, remarkable rate capability, and excellent electrochemical stability. Furthermore, we had fabricated symmetric supercapacitor to further assess the application value of $PANI_1$-coated graphite electrode, indicating that $PANI_1$ exhibited high energy and power density.

2. EXPERIMENTAL SECTION

Materials. Aniline (ANI) was chemically pure and used for polymerization without further purification. Ammonium persulfate (APS) was used as oxidizer in the reaction of polymerization. 37% hydrochloric acid (HCl) solution, 98% H_2SO_4 solution and ethanol absolute were analytical grade and were commercially obtained from Chain Medicine Co. Deionized water was used for all polymerization and testing experiments.

Preparation of the PANI Nanofibers. The $PANI_1$ thin film had deposited on graphite electrodes through microwave irradiation (G70D23AP-TD, 140−700 W, working frequency 2.45 GHz, Guangdong China) without controlling the reaction temperature. The typical synthesis procedure was as follows. The graphite electrodes with about 1.7 g (6 mm in diameter and 4 cm in length, spectral purity) were washed with double distilled water and ethanol absolute several times in the ultrasonic cleaner, respectively. The graphite electrodes were dried at 80 °C overnight before use. Then, as shown in Scheme 1, 12 mL HCl-ANI mixed solution was added into a glass beaker, in which the concentration of HCl was 1.25 M and volume ratio (VR) of ANI was 1%, 2%, 3%, 4% and 5%, respectively. PANI was prepared by ANI oxidation in the presence of APS (0.2 g). The microwave-assisted synthesis was carried out for 2 min in the power of 700 W. The graphite electrode was disposed in the same way in the solution without ANI as the comparison. The obtained electrodes were washed with double distilled water and ethanol absolute, respectively, and finally dried at 80 °C overnight.

Characterization. The morphology of $PANI_1$ was observed on field emission scanning electron microscopy (FE-SEM, Hitachi S-4800, Tokyo, Japan) and the transmission electron microscope (TEM, FEI Tecnai G20, USA). X-ray powder diffraction (XRD) was conducted on a TD-3500 XRD (Tongda Instrument Co., Dan-dong, China) with Cu Kα radiation source. The surface chemistry of $PANI_1$ and PANI in the solution under microwave radiation ($PANI_2$) were analyzed using Fourier transform infrared spectra (FT-IR, Suger Land 6700, TX, USA), Raman spectra using a Renishaw Raman System-Model 1000 spectrometer with 785 nm (red) laser excitation and X-ray photoelectron spectroscopy (XPS, Kratos AXIS 165, Shimadzu, Japan). The mass spectra were measured using a Bruker Ultraflex MALDI-TOF/TOF-MS (Bruker Daltonic GmbH, Bremen, Germany).

Electrochemical Measurements. CV, galvanostatic charge/discharge and EIS tests were conducted on an Autolab PGSTAT/FRA2 302 electrochemical workstation (Eco Chemie B.V., Amster-

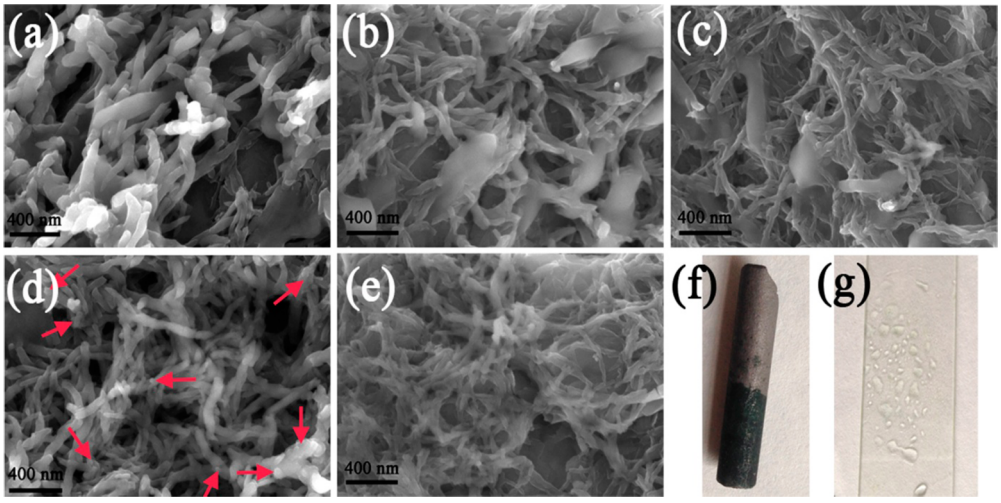

Figure 1. FE-SEM micrographs of $PANI_1$ at the different VRs of ANI in mixed solution, (a) 1, (b) 2, (c) 3, and (d) 4%, in which the red arrows are corresponding to the protuberances on the surface of $PANI_1$ nanofibers, and (e) 5%. The digital photograph of (f) $PANI_1$-coated graphite electrode and (g) vapor of reaction solution on glass by microwave-assisted heating.

dam, Netherlands). All the three-electrode electrochemical measurements were carried out at ambient temperature with a $PANI_1$-coated graphite electrode, a graphite sheet and saturated calomel electrode (SCE) served as the working electrode, counter electrode and reference electrode, respectively. The SC (F g^{-1}) from discharge curves is calculated[24] based on the relationship, $C = (It)/(Vm)$, where C, V, m, I, and t are designated as the total specific capacitance, operating voltage window, the mass of active material, the discharge current and the discharge time.

In a two-electrode system, two $PANI_1$-coated graphite electrodes with 2 mg active materials were constructed a symmetric electrochemical capacitor. The SC (F g^{-1}) of the electrodes, the energy density (E, Wh kg^{-1}) and power density (P, kW kg^{-1}) of capacitor from discharge curves are calculated[25] on the basis of the relationships $C = 4C_t$, $E = (1/8)CV^2$, and $P = (V - V_{drop})^2/(4MR)$, where C_t is the specific capacitance of symmetric supercapacitor, which is calculated from the equation of $C_t = (It)/(Vm)$, I (A) is the discharge current, t (s) is the discharge time, V (V) is the operating voltage window, M (g) is the total mass loading of both negative and positive electrodes, E is energy density, and P is the power density of the supercapacitor, and R is the internal resistance from IR drop obtained by the formula $R = (V_{drop})/(2I)$, where here V_{drop} (V) is the voltage drop at the beginning of the discharge and I (A) is the constant current.

3. RESULTS AND DISCUSSION

Pure PANI have really excellent theoretical SC[26] and may be higher than that, moreover, morphologies of PANI have a significant effect on the electrochemical properties. To achieve better electrochemical properties and good morphology of PANI nanofibers, we had designed a MCVI in situ polymerization method because of its advantages such as dramatic shrinkage in synthesis time, uniform heating and providing a force to form nanofibers structure, to easily and quickly deposit $PANI_1$ nanofibers onto the surface of graphite electrode. The possible formation process of $PANI_1$ nanofibers coated graphite electrode under microwave radiation is illustrated in Scheme 1a. The solution with ANI oligmer and APS is boiling to form acid mist during microwave-assisted heating. A polymerization reaction occurred on the graphite electrode surrounded by the acid mist. Figure 1f, g shows the digital photographs of $PANI_1$-coated graphite electrode and microwave vapor of reaction solution on glass, indicating that $PANI_1$ could commendably deposit on graphite electrode using our method.

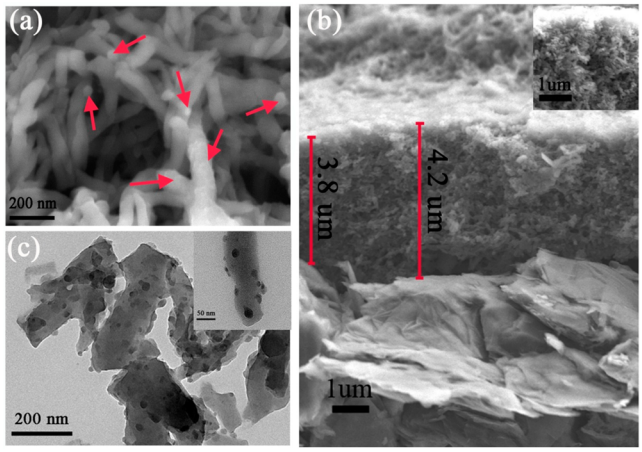

Figure 2. FE-SEM and TEM micrographs of $PANI_1$. (a) FE-SEM of $PANI_1$ at 4%, the red arrows are corresponding to the protuberances on the surface of $PANI_1$ nanofibers. (b) Cross-sectional image of $PANI_1$-coated graphite electrode, the inset image is the profile morphology of $PANI_1$ nanofibers and (c) the TEM image of $PANI_1$, the inset image is the TEM image of nanofiber at 50 nm.

FE-SEM and TEM were used to determine the morphology of $PANI_1$ nanofibers. As shown in Figure 1a–e, the influence of VR of ANI in mixed solution on the morphology is investigated detailedly. All images show that the obtained $PANI_1$ is nanofiber-shaped. When the VR is 1% (Figure 1a), the nanofibers are short and thick. With the increasing of the VR, the nanofibers become gracile and denser. When the VR is 2% (Figure 1b), However, the nanofibers are with a part of agglomerate. The agglomerate nanofibers become less and less until completely disappear at 4% (Figure 1d), and the nanofibers are agglomerated again at 5% (Figure 1e). Because the nanofibers obtained at 4% are entangled, coarse and less compact, the VR of 4% is used for the subsequent study described in this paper.

Figure 2 further indicates the optimal morphology of $PANI_1$ nanofibers at 4%. As illustrated in Figure 2a, the FE-SEM image taken at high magnification further reveals fibrous structure with diameter from 50 to 100 nm. Furthermore, the cross-sectional image (Figure 2b) indicates that the $PANI_1$ nanofibers

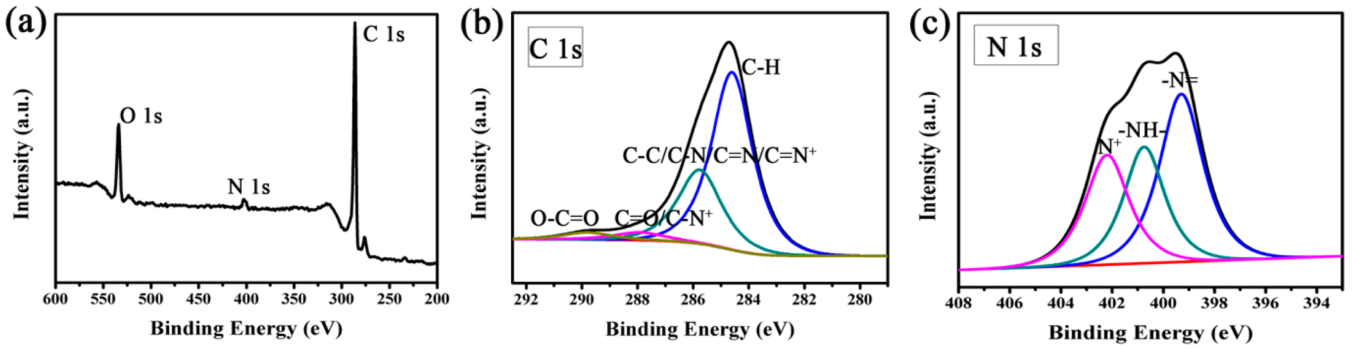

Figure 3. XPS spectra of $PANI_1$. (a) Wide scan survey, (b) C 1s spectrum, and (c) N 1s spectrum.

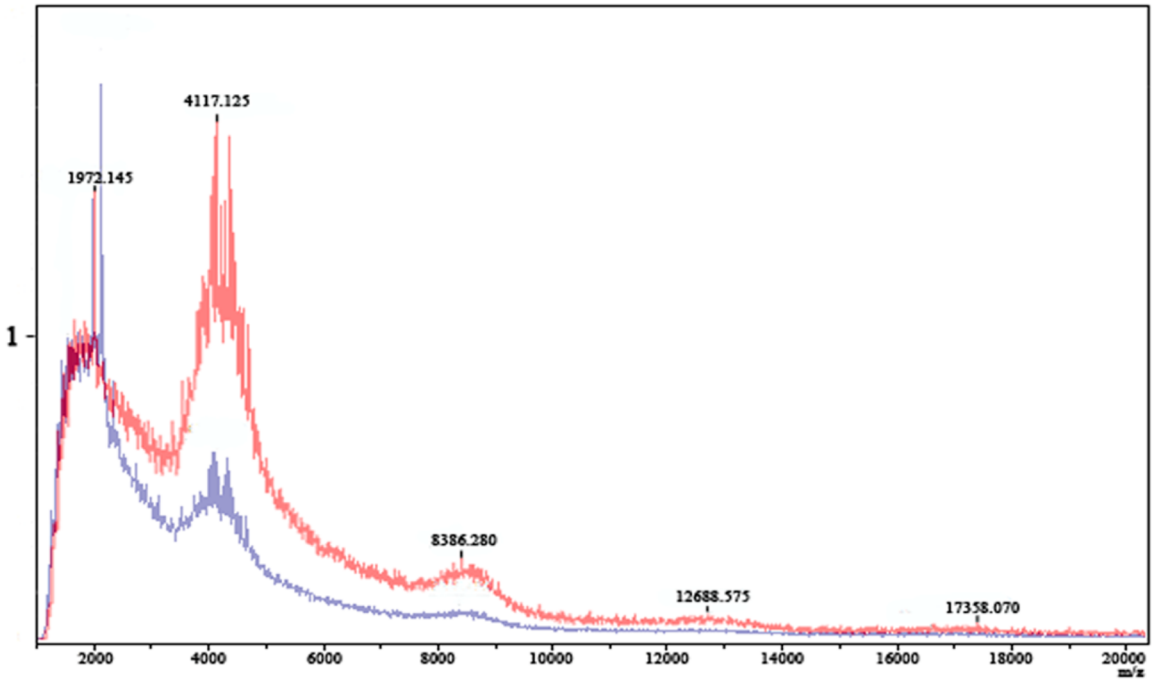

Figure 4. Normalization of MALDI-TOF spectra of $PANI_1$ (the red curve) and $PANI_2$ (the dark blue curve).

Scheme 2. Redox Reaction of PANI with Different States

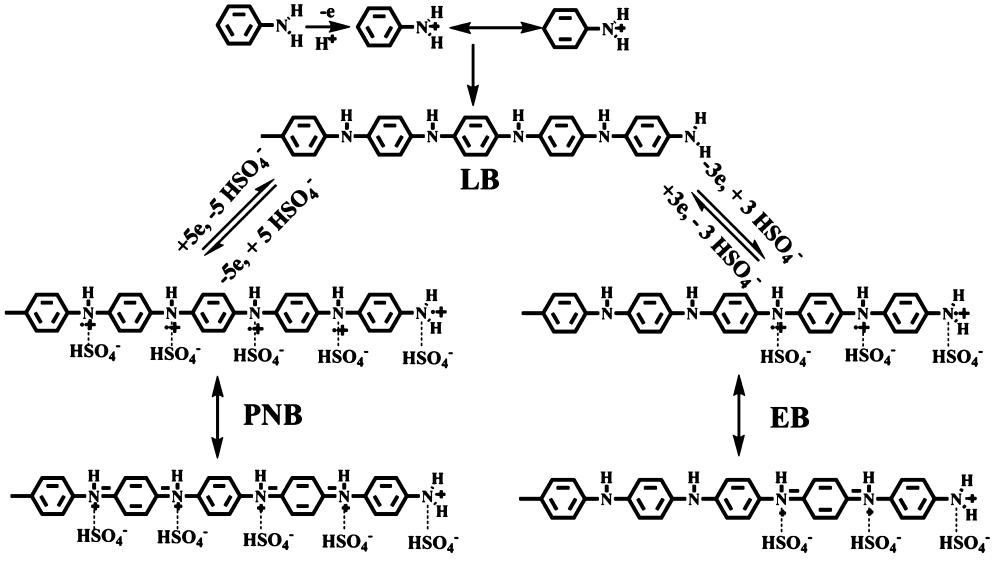

Scheme 3. Growth Schematic of (a) Long-Chain $PANI_1$ and the Redox Reaction in Solution and (b) $PANI_2$

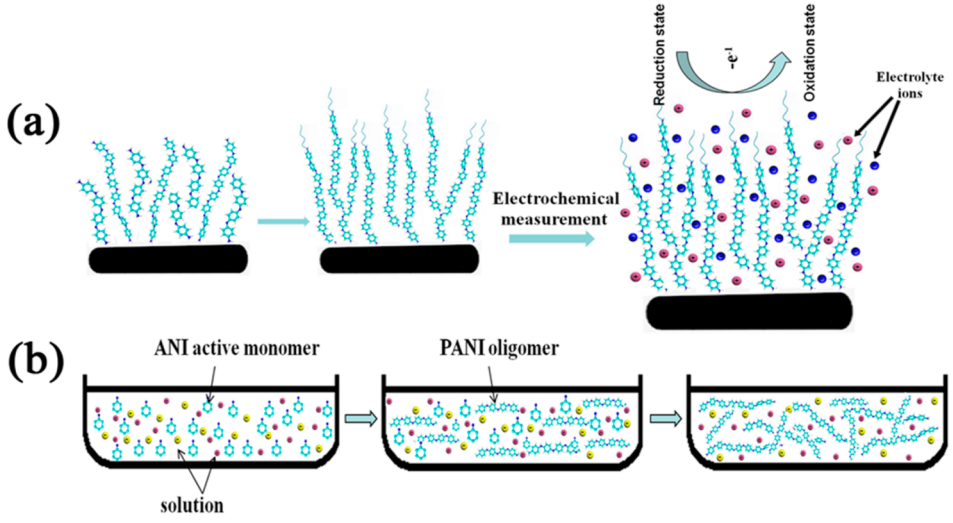

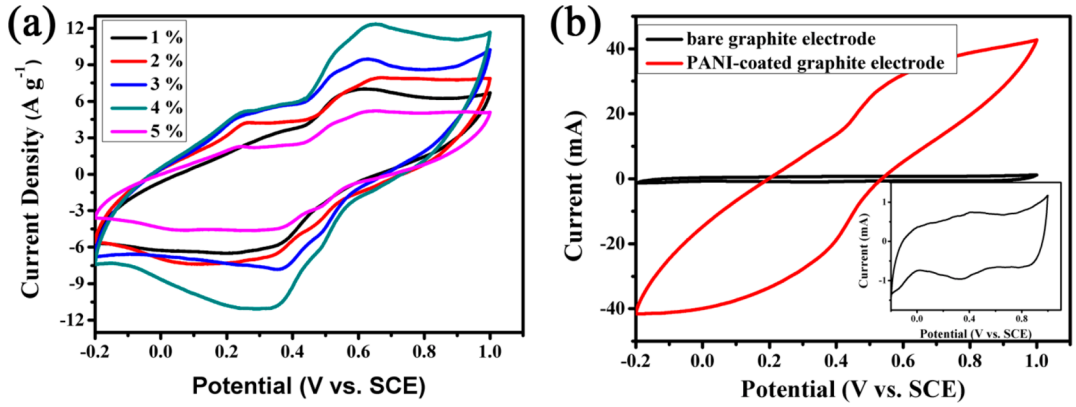

Figure 5. CV curves of (a) $PANI_1$-coated graphite electrode at the different VRs of ANI (1%, 2%, 3%, 4% and 5%) in 1 M H_2SO_4 electrolyte at scan rate of 10 mV s^{-1}, the mass of $PANI_1$ are 2.5, 2.8, 3.1, 3.0, and 2.6 mg, respectively. and (b) the comparison of bare graphite electrode and $PANI_1$-coated graphite electrode in 1 M H_2SO_4 electrolyte at scan rate of 10 mV s^{-1} (The inset image show an enlarged view of CV curve of bare graphite electrode).

film with the thickness of ~4 um are obtained and the inset image clearly reveals the profile morphology of nanofibers which are compact. Further investigation by TEM reveals that the obtained $PANI_1$ nanofibers are not smooth and have some protuberances on their surface (also clearly seen the red arrows of Figures 1d and 2a), which may depend on the nucleation and growth process of $PANI_1$, mainly including the secondary growth of $PANI_1$, which has been explained in detail later in this article. The protuberance on the surface of $PANI_1$ nanofibers may increase the connection and promote the electron transfer among the nanofibers during the electrochemical measurement, indicating that the obtained $PANI_1$ may be an optimal electrode material.

The chemical structures of $PANI_1$ and $PANI_2$ were analyzed by FTIR and Raman spectra. As shown in Figure S1 (see the Supporting Information), the new two characteristic peaks located at 1706.8 and 1303.2 cm^{-1} in $PANI_1$ corresponding to the stretching vibration of C═O and the deformation vibrations of C−O, respectively,[27] indicating that the carboxyl group is successfully introduced onto the surface of graphite electrode. The result was further proved by Raman spectra (see Figure S2 in the Supporting Information). Figure S3 in the Supporting Information shows the XRD image of $PANI_1$, two obvious peaks centered at 2θ = 20.9 and 26.3° are ascribed to the periodicity parallel and perpendicular to $PANI_1$ chains, respectively.[28,29] And the inset image indicates that the $PANI_1$ film have been successfully synthesized on the surface of graphite electrode.

To confirm the FTIR and XRD results, we further characterized the valence states of $PANI_1$ and $PANI_2$ with XPS spectra and the results are shown in Figure 3 and Figure S4 in the Supporting Information. Figure 3 shows the XPS spectra of $PANI_1$ in detail. Figure 3a shows the wide scan survey, in which the O 1s photoemission peak was clearly observed. Furthermore, The C 1s spectrum (Figure 3b) related to the surface functional groups on the graphite electrode can be decomposed into four subpeaks, which are attributed to the functional groups of $PANI_1$ (aromatic C−H at 284.600 eV and C−C/C−N/C═N/C═N^+ at 285.759 eV), and the surface functional group of graphite electrode (carbonyl C═O at 287.920 eV and the carboxyl O−C═O at 289.810 eV), respectively.[30,31] An N 1s spectrum (Figure 3c) is deconvoluted into three Gaussian peaks correlated to three different electronic states, namely, the quinoid amine (=N−) with Binding Energy (BE) at 399.300 eV, the benzenoid amine (−NH−) with BE at 400.750 eV, and the nitrogen cationic

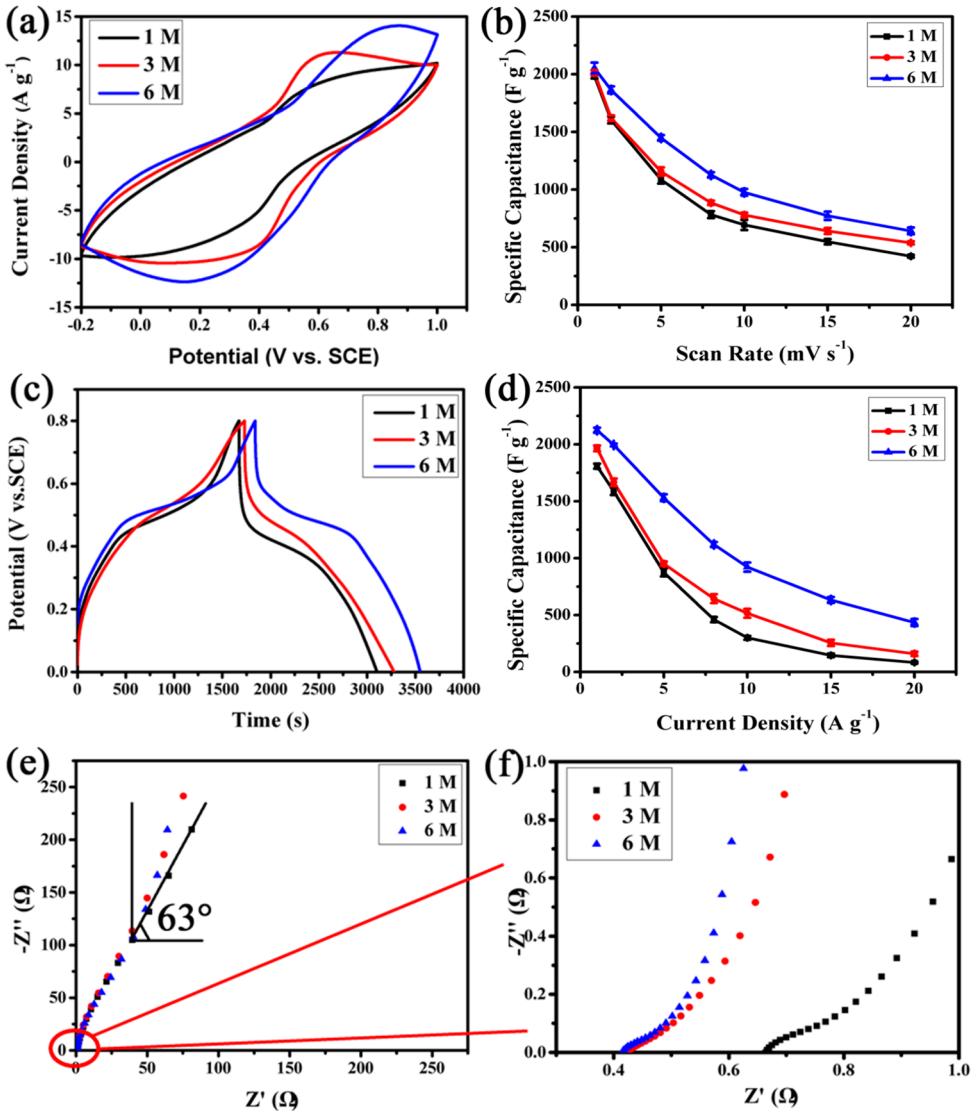

Figure 6. Electrochemical measurements of $PANI_1$–coated graphite electrode in 1, 3, and 6 M H_2SO_4 electrolytes in three-electrode system. (a) CV curves at the scan rate of 5 mV s^{-1} in the potential rang of −0.2 to 1.0 V vs SCE. (b) The corresponding SCs at various scan rates (1, 2, 5, 8, 10, 15, and 20 mV s^{-1}). (c) The galvanostatic charge–discharge curves at the current density of 1 A g^{-1}. (d) The corresponding SCs at various current densities (1, 2, 5, 8, 10, 15, and 20 A g^{-1}). (e) Nyquist plots from EIS measurements. (f) An enlarged portion of the low resistance region of EIS. The mass of $PANI_1$ are 3.6, 4.1, and 3.6 mg at measurements in 1, 3, and 6 M H_2SO_4 electrolytes, respectively.

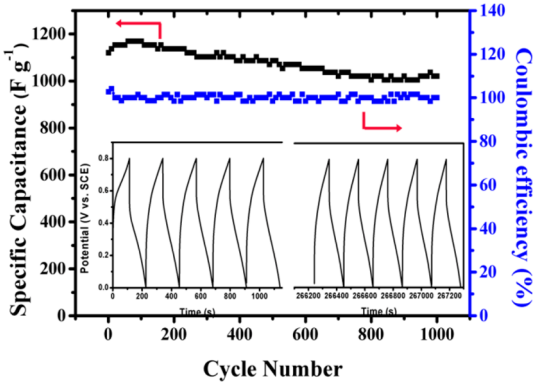

Figure 7. Cycling stability of $PANI_1$-coated graphite electrode at current density of 8 A g^{-1} in 6 M H_2SO_4 electrolyte in three-electrode system. The inset image shows the first and the last five cycles.

radical (N^+) with BE at 402.200 eV.[30,32] The results indicate that the $PANI_1$ has been obtained and the carboxyl is successfully formed in the surface of graphite electrode. Figure S4 in the Supporting Information shows the XPS spectrum of $PANI_2$, which corresponds to the N 1s spectrum of $PANI_1$.

The generally accepted structure of PANI is described as Scheme S1a in the Supporting Information,[33] where Y ($0 \leq Y \leq 1$) corresponds to the ratio of reduced unit and $1-Y$ corresponds to the ratio of oxidized unit in PANI. On account of the different value of Y, the states of PANI are different and mainly include three isolable oxidation–reduction states, which cover fully reduced form ($Y = 1$) designated as leucoemeraldine base (LB, Scheme S1b in the Supporting Information), half-oxidized and half-reduced form ($Y = 0.5$) designated as emeraldine base (EB, Scheme S1c in the Supporting Information), and fully oxidized form ($Y = 0$) designated as pernigraniline base (PNB, Scheme S1d in the Supporting Inforrmation). The atomic concentration of nitrogen in $PANI_1$ and in $PANI_2$ is shown in Table S1 in the Supporting

dx.doi.org/10.1021/am505533c | ACS Appl. Mater. Interfaces 2014, 6, 19978–19989

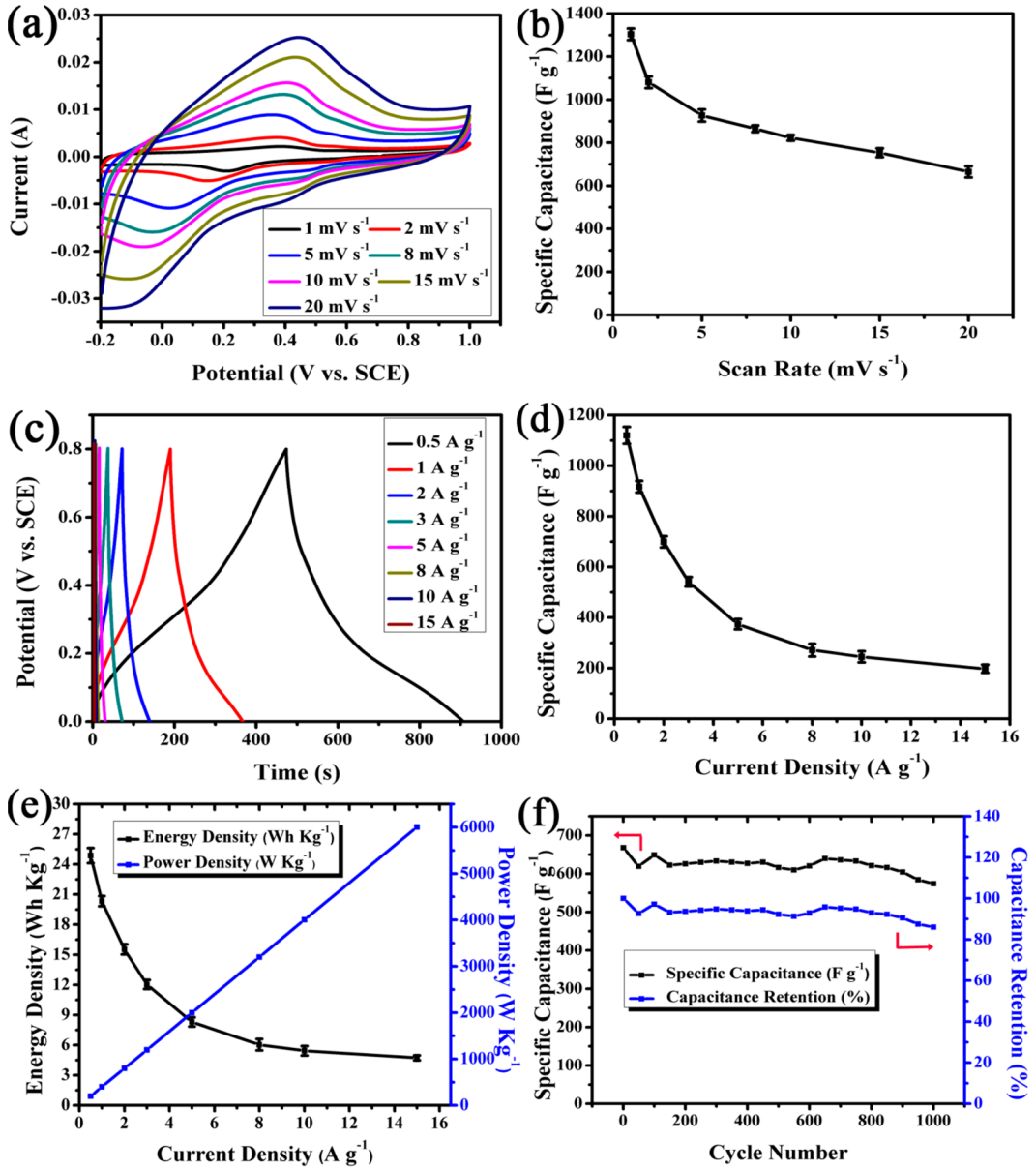

Figure 8. Electrochemical measurements of $PANI_1$-coated graphite electrode in 6 M H_2SO_4 electrolyte in two-electrode system. (a) CV curves at the different scan rates (1, 2, 5, 8, 10, 15, 20 mV s^{-1}). (b) Corresponding SCs at various scan rates. (c) Galvanostatic charge−discharge curves at different current densities (0.5, 1, 2, 5, 8, 10, 15 A g^{-1}). (d) Corresponding SCs at various current densities. (e) Ragone plot of $PANI_1$−coated graphite electrode. (f) Cycling stability of the $PANI_1$-coated graphite electrode symmetric supercapacitor at a scan rate of 20 mV s^{-1}.

Information, the amount of =N−, −NH− and N+ are 43.44, 28.18, and 28.37% in $PANI_1$, and 59.22, 13.55, and 27.23% in $PANI_2$, respectively. According to the results, the predominant atomic structures both in $PANI_1$ and in $PANI_2$ are =N−. And the mixed structure of EB and PNB mainly exist in our obtained PANI ($0 < Y < 0.5$), indicating that the obtained PANI has more quinoid structures which could present a large affinity for high mobility charges.[34] However, the concentration of =N− in $PANI_2$ is higher than that of in $PANI_1$, indicating that $PANI_2$ contains more oxidation state components because ANI oligomer has highly contacted with oxidizing agent in solution and promotes $PANI_2$ to be further oxidized during reaction, resulting in the concentration of PNB in $PANI_1$ being lower than that in $PANI_2$. As we know, the conductivity of PNB is quite poor,[35] indicating that $PANI_1$ may be an optimal material to present better electrical conductivity.

The MALDI−TOF analysis of $PANI_1$ and $PANI_2$ are shown in Figure 4. The peaks of the mass spectra of $PANI_1$ and $PANI_2$ studied are grouped in multiplets, which imply the presence in the segments of PANI structures. Obviously, the intensity of peaks in $PANI_1$ at higher molecule mass is stronger than that in $PANI_2$, indicating that a larger relatively percentage composition of high molecular mass exist in $PANI_1$. For linear PANI, degree of polymerization is one of the key parameters, which is proportional to chain-length. The MALDI-TOF results indicate that $PANI_1$ has higher relatively percentage composition of high degree of polymerization than $PANI_2$, illustrating that $PANI_1$ contains a greater number of long chains. High linear charge density could be produced on the polymer chain during redox. However, this high charge density must have coupling charge to stabilize. $PANI_1$ with longer chains can provide more coupling charge and may be beneficial to improve the ability to

keep electron stability, thus forms a more stable and higher electroactive chemical structure (Scheme 2). As is commonly known, the pseudocapacitance of PANI comes from the redox reaction involving the doping and dedoping of counter-anions (HSO_4^-) from the electrolyte, accompanying the change of electrons of nitrogen atom (Scheme 2). And the high content of nitrogen atom in $PANI_1$ nanofibers at the unit mass resulting from its longer chain of $PANI_1$ can promote the protonation of $PANI_1$ and then improve the redox reaction (Scheme 3a). Furthermore, the smaller quantity of chains in unit mass of $PANI_1$ can decrease the electron transfer resistance. It can be reckoned that $PANI_1$ nanofibers with fine entangled and loosened structures synthesized by MCVI in situ polymerization may be endowed with exciting electrochemical performance.

According to the results above, we propose the possible polymerization mechanism of $PANI_1$ by MCVI in situ polymerization method. As shown in Scheme 1a, the surface of graphite electrode is lamellar structure and the layers strongly absorb microwave radiation until become hot and fluffy during microwave-assisted heating. Meanwhile, the surface of graphite is modified with carboxyl (negative) in acid mist with ANI and APS (proved by FT-IR and XPS images), which can provide a certain number of active sites for nucleation or polymerization of ANI (Scheme 1b). Then, the $PANI_1$ is obtained by ANI monomer polymerization, which is positive in the acid. Thus, because of electrostatic interaction between negative carboxyl and positive $PANI_1$, $PANI_1$ firmly grows on graphite electrode when the solution is boiling.[27] In addition, rapid exotherm of the hot graphite electrode when it is surrounded by the vapor is also an important factor to promote the better contact of the $PANI_1$ and the graphite electrode.

It is assumed that under optimum conditions, the ANI nuclei produce stacks stabilized by $\pi-\pi$ interactions between phenazine-containing oligomers.[14,36] ANI monomer nucleates and polymerizes under microwave radiation (Scheme 1c), and produce amount of active centers for growth of $PANI_1$ chains. However, the environment of polymerization may have a significantly greater influence on the number of active centers, and then effect the chain growth of $PANI_1$ (proved by MALDI-TOF analyze). According to Scheme 3a, ANI forms some oligomers active center on the graphite electrode and then easily grows to form long-chain $PANI_1$ because of the better linear nature of $PANI_1$ chains under microwave radiation. As we know, the initiator molecules are three-dimensionally mixed with the monomer molecules in bulk solution. Therefore, each molecule of the initiator is capable of creating a nucleation center for $PANI_2$ chain growth.[10] Therefore, a large number of active centers are formed in solution (Scheme 3b) and lots of oligomers are produced. The obtained oligomers could not be further polymerization sufficient in such a short time because of the effect of ion diffusion resistance in solution, leading to form amounts of short chains in $PANI_2$. Furthermore, accompanying the $PANI_1$ nanofibers are formed on the graphite electrode, new free nuclei adsorb on the nanofiber and continue growing on the surface, producing some protuberances on the surface of $PANI_1$ nanofibers because of the limit of polymerization time, which is called the secondary growth of PANI.[37] Moreover, irregular movement of molecules under microwave radiation causes the heterogeneous nucleation, which results in forming the coarse surface of nanofibers. As a result, the coarse $PANI_1$ nanofibers with some protuberances and longer chains come into being.

The MCVI in situ deposition of our $PANI_1$ nanofibers on graphite electrode provides a practical method to synthesis of nanostructures. Such nanostructure can provide a relatively short diffusion path for electrolyte ions to access the electroactive surface of $PANI_1$ and facilitate electron transfer fleetly between electrode and electrolyte, improving the electrochemical use of active materials. To evaluate the electrochemical performance of $PANI_1$ as active supercapacitor electrodes, we performed a combination of CV, galvanostatic charge−discharge, and EIS measurements in a conventional three-electrode system. CV is considered as an ideal tool in characterization the supercapacitive behavior of any material. Here, it was used to optimize the VR of ANI in mixed solution. The capacitive properties of the $PANI_1$-coated graphite electrode by changing VR of ANI were studied within the potential window of −0.2 to 1.0 V vs SCE in 1 M H_2SO_4 electrolyte at the scan rate of 10 mV s^{-1} and the corresponding results are shown in Figure 5a. The area enclosed by the CV curves increases with the VR of ANI from 1% to 4%, until the largest area is obtained at 4%. With the increasing of VR of ANI, the nanofibers become denser. This could provide more active sites. However, when the VR of ANI increases to 5%, the area enclosed by the CV curve is decreased. It may result from the disorderly and agglomerate $PANI_1$ obtained at 5% which could not be fully used for energy storage. The results prove that the $PANI_1$ obtained from the VR of ANI at 4% shows the optimal capacitive performance, which corresponds to the results from FE-SEM images (Figure 1).

To contrast the capacitive property of the substrate graphite electrode and the $PANI_1$-coated graphite electrode, we carried out CV curves at the same scan rate of 10 mV s^{-1} in 1 M H_2SO_4 electrolyte. As shown in Figure 5b, the shape of the CV curves of $PANI_1$-coated graphite electrode and bare graphite electrode has substantial discrepancy and the area enclosed by CV curve of the former is much greater than that of the latter. The CV curve of bare graphite electrode exhibits a double-layer capacitance characteristic (shown in the inset image of Figure 5b), which corresponds to the carbon material, indicating that it has no effect on the shape and peak intensity of $PANI_1$-coated graphite electrode. As a result, the graphite substrate contributing to the whole capacitance of $PANI_1$-coated graphite electrode is negligible.

To evaluate the influence of concentration of electrolyte on the electrochemical properties of $PANI_1$, we performed electrochemical measurement in detail in three different concentrations of H_2SO_4 electrolyte (1, 3, and 6 M) in three-electrode system and the corresponding results are shown in Figure 6. Figure 6a shows the CV curves at a scan rate of 5 mV s^{-1}, which indicate that the $PANI_1$ shows the largest SC in 6 M H_2SO_4. Furthermore, the $PANI_1$ shows the best rate capability in 6 M H_2SO_4 electrolyte (Figure 6b). This material stores the energy based on the Faradaic pseudocapacitance. But only one couple of wide redox peaks of $PANI_1$ is observed, illustrating that the $PANI_1$ may have conformational defects and a free of structural,[38] which is caused by the microwave radiation having been strongly absorbed by the polar molecular of $PANI_1$ and further entering into the internal of $PANI_1$ molecular. Galvanostatic charge−discharge measurements are also taken at various current densities to analyze and predict the performance of our active $PANI_1$ under practical operating conditions. It can be seen that the curves are nearly linear and

symmetrical, which is another typical characteristic of an ideal capacitor. According to Figure 6c, the $PANI_1$ has the longest discharge time in current density of 1 A g^{-1} in 6 M H_2SO_4. Furthermore, the charge time and discharge time are nearly equal, indicating that the material shows an excellent Coulombic efficiency. Figure 6d shows the SC in three different concentrations of electrolytes at the various current densities from 1 to 20 A g^{-1}. The $PANI_1$ exhibited excellent SC of 2136 F g^{-1} in the current density of 1 A g^{-1} in 6 M H_2SO_4, and still keep as high as 425 F g^{-1} even at 20 A g^{-1}. However, the specific capacitance decreased from 1938 to 150 F g^{-1} in 3 M H_2SO_4 and from 1788 to 75 F g^{-1} in 1 M H_2SO_4 at the current densities from 1 to 20 A g^{-1}, respectively. The decrease in capacitance is primarily caused by the presence of inner active sites that cannot sustain the redox transitions completely at higher scan rate and current density. However, the higher the concentration of electrolyte, the larger the number of active ions are, which can promote the redox reaction more or less. This is why the $PANI_1$ exhibited more prominent rate capability with the increase of scan rate and current density in 6 M H_2SO_4. These results indicate that the $PANI_1$ has relatively best electrochemical property in 6 M H_2SO_4. Furthermore, the results of Figure S5 in the Supporting Information indicate that the optimal electrolyte concentration is 6 M.

The surface morphology and chemical structure of $PANI_1$ nanofibers after electrochemical test in 1, 3, and 6 M H_2SO_4 had analyzed by TEM (see Figure S6 in the Supporting Information), Raman (see Figure S7 in the Supporting Information), and XPS (see Figure S8 in the Supporting Information), respectively. The same surface morphology as previous has been found in Figure S6 in the Supporting Information. The Raman spectra show characteristic peaks of $PANI_1$ in Figure S7 in the Supporting Information. The content of element sulfur obviously increases after electrochemical test (see Figure S8 in the Supporting Information). Furthermore, the atomic content of nitrogen with different form in $PANI_1$ has undergone great changes (see Table S2 in the Supporting Information) because of the influence of the concentration of electrolyte and different ability to combine protons of the nitrogen with different form during electrochemical measurement. All the results indicate that the $PANI_1$ maintains previous structure after electrochemical measurement.

The electrochemical properties of $PANI_2$ had been investigated in 6 M H_2SO_4 in three-electrode system containing CV (see Figure S9a, b in the Supporting Information), galvanostatic charge−discharge (see Figure S9c, d in the Supporting Information). The SCs and rate capability are lower than $PANI_1$, indicating that the PANI shows better electrochemical properties in situ polymerization. Furthermore, the PANI nanofibers (see Figure S10 in the Supporting Information) have been successfully prepared on the graphite electrode by electrochemical in situ polymerization. As shown in Figure S11 in the Supporting Information, the electrochemical properties have been provided in detail in 6 M H_2SO_4 electrolyte in three-electrode system. The SCs and rate capability are also less than $PANI_1$, indicating that the PANI has better electrochemical property in MCVI in situ polymerization method in 6 M H_2SO_4.

It is of interest to compare our results with other reported SC values of PANI synthesized under various experimental conditions (see Table S3 in the Supporting Information).[7,9,13,39−59] According to this, several factors can be considered as responsible for the outstanding SC behavior of our $PANI_1$ nanofibers coated graphite electrode developed by the MCVI in situ polymerization method. First, it is the novel MCVI in situ synthesis method that causes some defects in the structure of nanofibers. Second, special nanofiber structure could promote the electron transfer between electrode and electrolyte. Third, the special valence states content of nitrogen in $PANI_1$, which present a large number of delocalized polarons with high content of quinoid structures. Fourth, a large concentration of nitrogen atoms existing at the long chain of $PANI_1$ resulting from the high polymerization degree of $PANI_1$ could promote the redox reaction.

EIS measurements were used for conductivity studies as well as to elucidate mechanism and kinetics of the chemical and electrochemical reactions on $PANI_1$-coated graphite electrode.[60] The Nyquist plot of $PANI_1$-coated graphite electrode between real (Z') and imaginary $(-Z'')$ part of impedance in three different concentrations of electrolytes are shown in Figure 6e. The nearly perpendicular shape of the obtained curve at lower frequencies indicates an ideal capacitive behavior of the electrodes. The minimum angle of 63° has been obtained in 1 M H_2SO_4 electrolyte and the slope is larger in 3 and 6 M H_2SO_4 than that in 1 M H_2SO_4 at low frequencies. The real-axis intercept at high frequency corresponds to the uncompensated resistance of the bulk-electrolyte solution, which is also known as R_{ESR}.[61] The magnitude of the R_{ESR} of $PANI_1$ in three different electrolytes is also obtained from the Z'-intercept as shown in Figure 6f. They are 0.66 Ω in 1 M H_2SO_4, 0.42 Ω in 3 M H_2SO_4, and 0.41 Ω in 6 M H_2SO_4, respectively. We notice that the R_{ESR} decreases with the increase of electrolyte concentration. This is attributed to the active points of contact between the material and electrolyte may increase in larger concentration of electrolyte, which could decrease the charge-transfer resistance at the interface between the electrode and the electrolyte. As shown in Figure 6f, the vertical curve has the largest slope with respect to the Z' axis in 6 M H_2SO_4, i.e., closest to the imaginary impedance axis $(-Z'')$, which implies that $PANI_1$-coated graphite electrode in 6 M H_2SO_4 exhibits the highest conductivity or lowest internal resistance, including polarization impedance. Furthermore, as we know, the semicircle arc in the high-frequency region might be attributed to diffusion effect of electrolyte in the electrode. The larger the semicircle arc, the higher the resistance of $PANI_1$-coated graphite electrode is. The small semicircle illustrates that the $PANI_1$ could be a desirable electrode material.

The detailed electrochemical properties of $PANI_1$-coated graphite electrode in 6 M H_2SO_4 were investigated containing CV (see Figure S12a in the Supporting Information), galvanostatic charge−discharge (see Figure S12b in the Supporting Information) and long-term cycle stability measurements in three-electrode system. Especially, the long-term cycle stability is one of the most important factors to consider for conducting polymers in supercapacitor applications. As can be seen in Figure 7, the electrochemical long-term cycle stability of the $PANI_1$-coated graphite electrode is investigated at a current density of 8 A g^{-1}. The capacitance of $PANI_1$-coated graphite electrode retained 91% of the initial capacitance after 1000 cycles. Interestingly, the SC is increases up to 1169 F g^{-1} from initial SC of 1120 F g^{-1} after 100 cycles, which may be explained with the better and better contact of $PANI_1$ with H_2SO_4 aqueous solution at the beginning of electrochemical measurement. The SC degradation may be caused by the combination of the effect of the collapse of nanofiber-shaped

$PANI_1$ and the shedding of $PANI_1$ from electrode more or less. This result is better than that of most of the electrode made by PANI nanostructure (see Table S3 in the Supporting Information). Therefore, the $PANI_1$-coated graphite electrode described in this work may be a potential candidate for supercapacitor applications with out-bound long-term cycle stability. Moreover, as shown in Figure 7, the constant charging/discharging experiments indicate that the electrode has a very stable Coulombic efficiency of ~100% over 1000 cycles. The inset image shows the first and the last five cycles at the cycling measurement. Such an excellent cyclability is thought to be related to the novel nanostructure of material composed of coarse and loosened $PANI_1$ nanofibers with some protuberances on, which can accommodate the big volume charge of $PANI_1$ during doping/dedoping processes. And the concentration of electrolyte is enough to maintain a better electrical and mechanical contact between electrode and electrolyte in 6 M H_2SO_4.

The symmetric supercapacitor was fabricated to further prove the electrochemical properties of $PANI_1$-coated graphite electrode. Figure 8a shows a set of CV curves at different scan rates varying from 1 to 20 mV s^{-1}. The CV curves also have one wide redox couple peak. The SC decrease from 1300 to 668 F g-1 at various scan rates (Figure 8b), showing excellent rate capability. Figure 8c depicts the profiles of galvanostatic charge−discharge measurements at various current densities varying from 0.5 to 15 A g^{-1}. The charge−discharge curves show good symmetry in the potential range, indicating that the supercapacitor has a high reversibility between charge and discharge processes. Figure 8c shows the SC of $PANI_1$-coated graphite electrode at different current densities. The $PANI_1$-coated graphite electrode can reach maximum SC of 1085 F g^{-1} at the current density of 0.5 A g^{-1}. The high SC is obtained although the rate capability needs to improve. The rate capability could be further improved by synthesis PANI composites such as PANI-graphene composite like reported literature.[62] Figure 8d shows the Ragone plot of our electrode. At a charge/discharge rate of 0.5 A g^{-1}, the energy density of $PANI_1$-coated graphite electrode can be as high as 24 Wh kg^{-1}. The largest power density (6000 W kg^{-1}) was obtained at the current density of 15 A g^{-1}.We also evaluate the long-term cycling stability of the $PANI_1$-coated graphite electrode symmetric capacitor by CV at a scan rate of 20 mV s^{-1} for 1000 cycles. As shown in Figure 8, the $PANI_1$-coated graphite electrode symmetric capacitor exhibit electrochemical stability with about 86% retention of the initial available specific capacitance after 1000 cycles.

4. CONCLUSIONS

We successfully fabricated $PANI_1$ nanofiber-coated graphite electrode in situ polymerization using an MCVI in situ deposition method we designed. The coarse $PANI_1$ nanofibers were obtained with diameters from 50 to 100 nm and with some protuberances on the surface. The possible in situ polymerization mechanism of $PANI_1$ was clarified reasonably. We researched the electrochemical properties of $PANI_1$-coated graphite electrodes in three different concentrations of electrolytes in a three-electrode system and they displayed optimal electrochemical performance in 6 M H_2SO_4 electrolyte, including a remarkable specific capacitance as high as 2136 F g^{-1} at a current density of 1 A g^{-1} and excellent rate capability and cycle performance, retaining 91% of its initial capacitance after 1000 cycles. Furthermore, a symmetric supercapacitor shows maximum energy density and power density of 24 Wh kg^{-1} and 6000 W kg^{-1}. All the evidence suggests that the electrochemical properties have been significantly improved using our facial synthesis method and the special structure of $PANI_1$, which was promising for further development of PANI nanomaterial-based electrochemical supercapacitors after improving the rate capability. The works to improve the rate capability by synthesis of PANI hybrids include carbon nanotube and grapheme, etc., has been carried out in our lab.

■ ASSOCIATED CONTENT

Ⓢ Supporting Information

Supporting Information contain FT-IR and Raman spectra of $PANI_1$ and $PANI_2$, XRD of $PANI_1$, N 1s XPS spectra of $PANI_2$, XPS atomic concentration of N 1s of $PANI_1$ and $PANI_2$, TEM, XPS and Raman spectra of $PANI_1$ and $PANI_2$ after electrochemical measurement, different states of PANI, electrochemical measurement of $PANI_2$ and PANI nanofibers in situ electrodeposition on graphite electrode, Galvanostatic charge−discharge curves of $PANI_1$-coated graphite electrode in 6 M H_2SO_4 and a comparison table about this work and the previous works. This material is available free of charge via the Internet at http://pubs.acs.org.

■ AUTHOR INFORMATION

Corresponding Author

*E-mail: xiaodan@scu.edu.cn. Tel: +86-28-85416029. Fax: +86-28-85415029.

Notes

The authors declare no competing financial interest.

■ ACKNOWLEDGMENTS

This work was financially supported by the National Natural Science Foundation of China (21177090 and 21275104).

■ REFERENCES

(1) Cuentas-Gallegos, A. K.; Lira-Cantú, M.; Casañ-Pastor, N.; Gómez-Romero, P. Nanocomposite Hybrid Molecular Materials for Application in Solid-State Electrochemical Supercapacitors. *Adv. Funct. Mater.* **2005**, *15*, 1125−1133.

(2) Hall, P. J.; Mirzaeian, M.; Fletcher, S. I.; Sillars, F. B.; Rennie, A. J. R.; Shitta-Bey, G. O.; Wilson, G.; Cruden, A.; Carter, R. Energy Storage in Electrochemical Capacitors: Designing Functional Materials to Improve Performance. *Energy Environ. Sci.* **2010**, *3*, 1238−1251.

(3) Vu, A.; Li, X.; Phillips, J.; Han, A.; Smyrl, W. H.; Bühlmann, P.; Stein, A. Three-Dimensionally Ordered Mesoporous (3DOm) Carbon Materials as Electrodes for Electrochemical Double-Layer Capacitors with Ionic Liquid Electrolytes. *Chem. Mater.* **2013**, *25*, 4137−4148.

(4) Li, S.; Wu, D.; Cheng, C.; Wang, J.; Zhang, F.; Su, Y.; Feng, X. Polyaniline-Coupled Multifunctional 2D Metal Oxide/Hydroxide Graphene Nanohybrids. *Angew. Chem., Int. Ed.* **2013**, *125*, 12327−12331.

(5) Chen, D.; Miao, Y. E.; Liu, T. Electrically Conductive Polyaniline/Polyimide Nanofiber Membranes Prepared via a Combination of Electrospinning and Subsequent in Situ Polymerization Growth. *ACS Appl. Mater. Interfaces* **2013**, *5*, 1206−1212.

(6) Mengqiang, W.; Liping, Z.; Dongmei, W.; Jiahui, G.; Shuren, Z. Electrochemical Capacitance of MWCNT/Polyaniline Composite Coatings Grown in Acidic MWCNT Suspensions by Microwave-assisted Hydrothermal Digestion. *Nanotechnology* **2007**, *18*, 385603−385603.

(7) Wu, Q.; Xu, Y.; Yao, Z.; Liu, A.; Shi, G. Supercapacitors Based on Flexible Graphene/Polyaniline Nanofiber Composite Films. *ACS Nano* **2010**, *4*, 1963−1970.

(8) Xie, K. Y.; Li, J.; Lai, Y. Q.; Zhang, Z. A.; Liu, Y. X.; Zhang, G. G.; Huang, H. T. Polyaniline Nanowire Array Encapsulated in Titania Nanotubes as a Superior Electrode for Supercapacitors. *Nanoscale* **2011**, *3*, 2202−2207.
(9) Pan, L. J.; Yu, G. H.; Zhai, D. Y.; Lee, H. R.; Zhao, W. T.; Liu, N.; Wang, H. L.; Tee, B. C. K.; Shi, Y.; Cui, Y.; Bao, Z. N. Hierarchical Nanostructured Conducting Polymer Hydrogel with High Electrochemical Activity. *Proc. Natl. Acad. Sci. U.S.A.* **2012**, *109*, 9287−9292.
(10) Huang, J.; Kaner, R. B. A General Chemical Route to Polyaniline Nanofibers. *J. Am. Chem. Soc.* **2003**, *126*, 851−855.
(11) Qunwei, T.; Xiaoming, S.; Qinghua, L.; Jihuai, W.; Jianming, L.; Miaoliang, H. Synthesis of Oriented Polyaniline Flake Arrays. *Mater. Lett.* **2009**, *63*, 540−542.
(12) Yu, L.; Bichen, W.; Wei, F. Chiral Polyaniline with Flaky, Spherical and Urchin-like Morphologies Synthesized in the L-phenylalanine Saturated Solutions. *Synth. Met.* **2009**, *159*, 1597−1602.
(13) Wang, Y. G.; Li, H. Q.; Xia, Y. Y. Ordered Whiskerlike Polyaniline Grown on the Surface of Mesoporous Carbon and Its Electrochemical Capacitance Performance. *Adv. Mater.* **2006**, *18*, 2619−2623.
(14) Stejskal, J.; Sapurina, I.; Trchová, M. Polyaniline Nanostructures and the Role of Aniline Oligomers in their Formation. *Prog. Polym. Sci.* **2010**, *35*, 1420−1481.
(15) Yan, Y.; Deng, K.; Yu, Z.; Wei, Z. Tuning the Supramolecular Chirality of Polyaniline by Methyl Substitution. *Angew. Chem., Int. Ed.* **2009**, *121*, 2037−2040.
(16) Tran, H. D.; Li, D.; Kaner, R. B. One-Dimensional Conducting Polymer Nanostructures: Bulk Synthesis and Applications. *Adv. Mater.* **2009**, *21*, 1487−1499.
(17) Wu, C.-G.; Bein, T. Conducting Polyaniline Filaments in a Mesoporosu Channel hos. *Science* **1994**, *264*, 1757−1759.
(18) Wei, Z.; Zhang, Z.; Wan, M. Formation Mechanism of Self-Assembled Polyaniline Micro/Nanotubes. *Langmuir* **2002**, *18*, 917−921.
(19) Su, F.; Miao, M.; Niu, H.; Wei, Z. Gamma-Irradiated Carbon Nanotube Yarn as Substrate for High-Performance Fiber Supercapacitors. *ACS Appl. Mater.Iinterfaces* **2014**, *6*, 2553−2560.
(20) Zhang, D.; Miao, M.; Niu, H.; Wei, Z. Core-Spun Carbon Nanotube Yarn Supercapacitors for Wearable Electronic Textiles. *ACS Nano* **2014**, *8*, 4571−4579.
(21) Cong, H.-P.; Ren, X.-C.; Wang, P.; Yu, S.-H. Flexible Graphene−Polyaniline Composite Paper for High-Performance Supercapacitor. *Energy Environ. Sci.* **2013**, *6*, 1185−1191.
(22) Chandrasoma, A.; Grant, R.; Bruce, A. E.; Bruce, M. R. M. Electrochemical Polymerization of Aniline on Carbon-Aluminum Electrodes for Energy Storage. *J. Power Sources* **2012**, *219*, 285−291.
(23) Wang, K.; Meng, Q.; Zhang, Y.; Wei, Z.; Miao, M. High-Performance Two-Ply Yarn Supercapacitors Based on Carbon Nanotubes and Polyaniline Nanowire Arrays. *Adv. Mater.* **2013**, *25*, 1494−1498.
(24) Zhao, X.; Zhang, L. L.; Murali, S.; Stoller, M. D.; Zhang, Q. H.; Zhu, Y. W.; Ruoff, R. S. Incorporation of Manganese Dioxide within Ultraporous Activated Graphene for High-Performance Electrochemical Capacitors. *ACS Nano* **2012**, *6*, 5404−5412.
(25) He, S.; Wei, J.; Guo, F.; Xu, R.; Li, C.; Cui, X.; Zhu, H.; Wang, K.; Wu, D. A Large Area, Flexible Polyaniline/Buckypaper Composite with a Core−Shell Structure for Efficient Supercapacitors. *J. Mater. Chem. A* **2014**, *2*, 5898−5902.
(26) Li, H.; Wang, J.; Chu, Q.; Wang, Z.; Zhang, F.; Wang, S. Theoretical and Experimental Specific Capacitance of Polyaniline in Sulfuric Acid. *J. Power Sources* **2009**, *190*, 578−586.
(27) Jian, C.; Hamon, M. A.; Hui, H.; Yongsheng, C.; Rao, A. M.; Eklund, P. C.; Haddon, R. C. Solution Properties of Single-Walled Carbon Nanotubes. *Science* **1998**, *282*, 95−98.
(28) Zhang, L.; Wan, M. Self-Assembly of Polyaniline—From Nanotubes to Hollow Microspheres. *Adv. Funct. Mater.* **2003**, *13*, 815−820.
(29) Yang, Y. S.; Wan, M. X. Chiral Nanotubes of Polyaniline Synthesized by a Template-Free Method. *J. Mater. Chem.* **2002**, *12*, 897−901.
(30) Zhong, M.; Song, Y.; Li, Y.; Ma, C.; Zhai, X.; Shi, J.; Guo, Q.; Liu, L. Effect of Reduced Graphene Oxide on the Properties of an Activated Carbon Cloth/Polyaniline Flexible Electrode for Supercapacitor Application. *J. Power Sources* **2012**, *217*, 6−12.
(31) Lee, S. W.; Kim, B.-S.; Chen, S.; Shao-Horn, Y.; Hammond, P. T. Layer-by-Layer Assembly of All Carbon Nanotube Ultrathin Films for Electrochemical Applications. *J. Am. Chem. Soc.* **2008**, *131*, 671−679.
(32) Hyder, M. N.; Lee, S. W.; Cebeci, F. Ç.; Schmidt, D. J.; Shao-Horn, Y.; Hammond, P. T. Layer-by-Layer Assembled Polyaniline Nanofiber/Multiwall Carbon Nanotube Thin Film Electrodes for High-Power and High-Energy Storage Applications. *ACS Nano* **2011**, *5*, 8552−8561.
(33) Deng, H.; Van Berkel, G. J.; Takano, H.; Gazda, D.; Porter, M. D. Electrochemically Modulated Liquid Chromatography Coupled On-Line with Electrospray Mass Spectrometry. *Anal. Chem.* **2000**, *72*, 2641−2647.
(34) Wohlgenannt, M.; Jiang, X.; Vardeny, Z. Confined and Delocalized Polarons in π-Conjugated Oligomers and Polymers: A Study of the Effective Conjugation Length. *Phys. Rev. B* **2004**, *69*, 241204(1)−241204(4).
(35) Kolla, H. S.; Surwade, S. P.; Zhang, X.; MacDiarmid, A. G.; Manohar, S. K. Absolute Molecular Weight of Polyaniline. *J. Am. Chem. Soc.* **2005**, *127*, 16770−16771.
(36) Zhou, C. F.; Du, X. S.; Liu, Z.; Ringer, S. P.; Mai, Y. W. Solid Phase Mechanochemical Synthesis of Polyaniline Branched Nanofibers. *Synth. Met.* **2009**, *159*, 1302−1307.
(37) Huang, J.; Kaner, R. B. A General Chemical Route to Polyaniline Nanofibers. *J. Am. Chem. Soc.* **2004**, *126*, 851−855.
(38) Montilla, F.; Cotarelo, M. A.; Morallón, E. Hybrid Sol−Gel−Conducting Polymer Synthesised by Electrochemical Insertion: Tailoring the Capacitance of Polyaniline. *J. Mater. Chem.* **2009**, *19*, 305−310.
(39) Li, Z.-F.; Zhang, H.; Liu, Q.; Liu, Y.; Stanciu, L.; Xie, J. Covalently-Grafted Polyaniline on Graphene Oxide Sheets for High Performance Electrochemical Supercapacitors. *Carbon* **2014**, *71*, 257−267.
(40) Gao, Z.; Wang, F.; Chang, J.; Wu, D.; Wang, X.; Wang, X.; Xu, F.; Gao, S.; Jiang, K. Chemically Grafted Graphene-Polyaniline Composite for Application in Supercapacitor. *Electrochim. Acta* **2014**, *133*, 325−334.
(41) Sk, M. M.; Yue, C. Y. Synthesis of Polyaniline Nanotubes Using the Self-Assembly Behavior of Vitamin C: a Mechanistic Study and Application in Electrochemical Supercapacitors. *J. Mater. Chem. A* **2014**, *2*, 2830−2038.
(42) Dhibar, S.; Das, C. K. Silver Nanoparticles Decorated Polyaniline/Multiwalled Carbon Nanotubes Nanocomposite for High-Performance Supercapacitor Electrode. *Ind. Eng. Chem. Res.* **2014**, *53*, 3495−3508.
(43) Yu, P.; Li, Y.; Zhao, X.; Wu, L.; Zhang, Q. Graphene-Wrapped Polyaniline Nanowire Arrays on Nitrogen-Doped Carbon Fabric as Novel Flexible Hybrid Electrode Materials for High-Performance Supercapacitor. *Langmuir* **2014**, *30*, 5306−5313.
(44) Mu, J.; Ma, G.; Peng, H.; Li, J.; Sun, K.; Lei, Z. Facile Fabrication of Self-Assembled Polyaniline Nanotubes Doped with D-Tartaric Acid for High-Performance Supercapacitors. *J. Power Sources* **2013**, *242*, 797−802.
(45) Peng, H.; Ma, G.; Ying, W.; Wang, A.; Huang, H.; Lei, Z. In Situ Synthesis of Polyaniline/Sodium Carboxymethyl Cellulose Nanorods for High-Performance Redox Supercapacitors. *J. Power Sources* **2012**, *211*, 40−45.
(46) Li, Y.; Zhang, Q.; Zhao, X.; Yu, P.; Wu, L.; Chen, D. Enhanced Electrochemical Performance of Polyaniline/Sulfonated Polyhedral Oligosilsesquioxane Nanocomposites with Porous and Ordered Hierarchical Nanostructure. *J. Mater. Chem.* **2012**, *22*, 1884−1892.

(47) Shaikh, S. F.; Lim, J. Y.; Mane, R. S.; Han, S.-H.; Ambade, S. B.; Joo, O.-S. Wet-Chemical Polyaniline Nanorice Mass-Production for Electrochemical Supercapacitors. *Synth. Met.* **2012**, *162*, 1303−1307.
(48) Deshmukh, P. R.; Pusawale, S. N.; Jamadade, V. S.; Patil, U. M.; Lokhande, C. D. Microwave Assisted Chemical Bath Deposited Polyaniline Films for Supercapacitor Application. *J. Alloys Compd.* **2011**, *509*, 5064−5069.
(49) Xie, K.; Li, J.; Lai, Y.; Zhang, Z. a.; Liu, Y.; Zhang, G.; Huang, H. Polyaniline Nanowire Array Encapsulated in Titania Nanotubes as a Superior Electrode for Supercapacitors. *Nanoscale* **2011**, *3*, 2202−2207.
(50) Li, Y.; Zhao, X.; Xu, Q.; Zhang, Q.; Chen, D. Facile Preparation and Enhanced Capacitance of the Polyaniline/Sodium Alginate Nanofiber Network for Supercapacitors. *Langmuir* **2011**, *27*, 6458−6463.
(51) Li, G.-R.; Feng, Z.-P.; Zhong, J.-H.; Wang, Z.-L.; Tong, Y.-X. Electrochemical Synthesis of Polyaniline Nanobelts with Predominant Electrochemical Performances. *Macromolecules* **2010**, *43*, 2178−2183.
(52) Liu, J.; Zhou, M.; Fan, L.-Z.; Li, P.; Qu, X. Porous Polyaniline Exhibits Highly Enhanced Electrochemical Capacitance Performance. *Electrochim. Acta* **2010**, *55*, 5819−5822.
(53) Wang, K.; Huang, J.; Wei, Z. Conducting Polyaniline Nanowire Arrays for High Performance Supercapacitors. *J. Phys. Chem. C* **2010**, *114*, 8062−8067.
(54) Zhang, H.; Li, H.; Zhang, F.; Wang, J.; Wang, Z.; Wang, S. Polyaniline Nanofibers Prepared by a Facile Electrochemical Approach and their Supercapacitor Performance. *J. Mater. Res.* **2011**, *23*, 2326−2332.
(55) Mondal, S. K.; Barai, K.; Munichandraiah, N. High Capacitance Properties of Polyaniline by Electrochemical Deposition on a Porous Carbon Substrate. *Electrochim. Acta* **2007**, *52*, 3258−3264.
(56) Zhou, H.; Chen, H.; Luo, S.; Lu, G.; Wei, W.; Kuang, Y. The Effect of the Polyaniline Morphology on the Performance of Polyaniline Supercapacitors. *J. Solid State Electrochem.* **2005**, *9*, 574−580.
(57) Prasad, K. R.; Munichandraiah, N. Electrochemical Studies of Polyaniline in a Gel Polymer Electrolyte. *Electrochem. Solid-State Lett.* **2002**, *5*, A271−A274.
(58) Prasad, K. R.; Munichandraiah, N. Fabrication and Evaluation of 450 F Electrochemical Redox Supercapacitors Using Inexpensive and High-Performance, Polyaniline Coated, Stainless-Steel Electrodes. *J. Power Sources* **2002**, *112*, 443−451.
(59) Fusalba, F.; Gouérec, P.; Villers, D.; Bélanger, D. Electrochemical Characterization of Polyaniline in Nonaqueous Electrolyte and Its Evaluation as Electrode Material for Electrochemical Supercapacitors. *J. Electrochem. Soc.* **2001**, *148*, A1−A6.
(60) Choi, B. G.; Hong, J.; Hong, W. H.; Hammond, P. T.; Park, H. Facilitated Ion Transport in All-Solid-State Flexible Supercapacitors. *ACS Nano* **2011**, *5*, 7205−7213.
(61) Chen, J.; Sheng, K.; Luo, P.; Li, C.; Shi, G. Graphene Hydrogels Deposited in Nickel Foams for High-Rate Electrochemical Capacitors. *Adv. Mater.* **2012**, *24*, 4569−4573.
(62) Yu, P.; Zhao, X.; Huang, Z.; Li, Y.; Zhang, Q. Freestanding Three-Dimensional Graphene and Polyaniline Nanowire Arrays Hybrid Foams for High-Performance Flexible and Lightweight Supercapacitors. *J. Mater.Chem. A* **2014**, *2*, 14413−14420.